Letter to editor

Sulfur-rich antimonselite, Sb$_2$(Se,S)$_3$ in the Se-bearing mineral association from the Příbram uranium and base metal ore district, Czech Republic

Pavel ŠKÁCHA[1, 2*], Jakub PLÁŠIL[3], Jiří SEJKORA[4], Viktor GOLIÁŠ[2]

[1] *Mining Museum Příbram, Hynka Kličky Place 293, 261 01 Příbram VI – Březové Hory, Czech Republic; skacha-p@muzeum-pribram.cz*
[2] *Institute of Geochemistry, Mineralogy and Mineral Resources, Faculty of Science, Charles University in Prague, Albertov 6, 128 43 Prague 2, Czech Republic*
[3] *Institute of Physics ASCR, v.v.i., Na Slovance 2, 182 21 Prague 8, Czech Republic*
[4] *Department of Mineralogy and Petrology, National Museum, Cirkusová 1740, 193 00 Prague 9-Horní Počernice, Czech Republic*
*Corresponding author

Antimonselite from the new occurrence, Příbram uranium–base metal ore district (Central Bohemia, Czech Republic), has been studied by means of electron microprobe and X-ray diffraction. Antimonselite crystals, reaching up to 1.5 mm across, were rarely found in the calcite gangue with uraninite in association with clausthalite, tiemannite, hakite, tetrahedrite, Se-rich chalcopyrite, permingeatite, Se-rich and Se-analogue of chalcostibite and dzharkenite. Based on electron-microprobe analyses, the empirical formula of the studied antimonselite (mean of 7 point analyses, recalculated to 5 *apfu)* is (Sb$_{2.06}$Cu$_{0.01}$)$_{\Sigma2.07}$(Se$_{2.47}$S$_{0.46}$)$_{\Sigma2.93}$. The studied S-rich antimonselite is orthorhombic, the space group *Pnma*, with *a* = 11.7156(3), *b* = 3.9514(11), *c* = 11.5645(3) Å, *V* = 535.36(15) Å^3, and *Z* = 4. The structure was refined from the single-crystal X-ray data to *R*$_1$ = 0.0143 for 634 reflections [with *I*$_{obs}$ > 3σ(*I*)]. The structure of S-rich antimonselite is isotypic to that of stibnite. Sulfur was found to be entering the selenium sites regularly without any evidence of preferential ordering of the atoms at the different sites.

1. Introduction

Antimonselite, ideally, Sb$_2$Se$_3$, is a rare Se-analogue of stibnite, Sb$_2$S$_3$, which has been described only from the several localities in China up to date. The mineral is known from localities Laerma (Wen et al. 2006) and Qiongmo (Liu et al. 1998), which are genetically related to Au–Se deposits. Other occurrences of antimonselite in the same country were found at uranium deposits: Baimadong (Chen et al. 1993), Sanqilinyi and Sanbaqi (Min and Wu 1992) and Bentou (Min et al. 1995).

Here, we describe the first occurrence of antimonselite in the Czech Republic. It was found in the association of other selenides and sulfides in the uranium-bearing veins of the Příbram uranium–base metal ore district (Růžička 1986). Two small fragments of calcite vein, containing the later analyzed antimonselite, were collected by one of the authors (PS) at the dump of the former uranium mine No. 16 (the Příbram–Háje deposit). In the current paper we present the new crystal structure data for the sulfur-rich variety of antimonselite.

2. Occurrence and sample description

The uranium and base-metal ore-district Příbram (Central Bohemia, Czech Republic) is located at an exocontact of the Central Bohemian Plutonic Complex with the Teplá–Barrandian Unit (Tvrdý 2003). Uranium mineralization occurs in a zone that is about 25 km long and up to 2 km wide and is concentrated in several separated ore deposits (Ettler et al. 2010). Selenium mineralization in the Příbram area was first mentioned by Růžička (1986) and later was studied by Litochleb et al. (2004), who described several selenide minerals from a historical specimen found during 1950's. Larger number of samples containing selenide mineralization (e.g. clausthalite, hakite, permingeatite, eskebornite) was recently found in the dump material from the shafts no. 11A Bytíz and no. 16 Háje (Škácha and Sejkora 2007; Škácha et al. 2009, 2010, 2014). The origin of selenide mineralization within the carbonate veins follows the crystallization of uraninite, while the redox potential of hydrothermal fluids is lowered and fugacity of Se increases (Dymkov 1985).

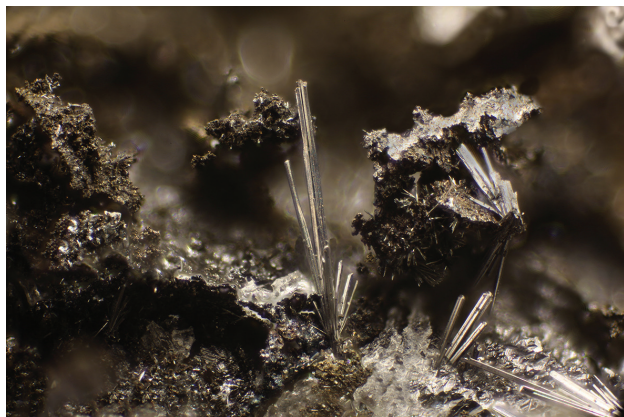Recently studied specimens containing antimonselite come from a dump material of the former uranium mine

Fig. 1 Antimonselite crystals etched from calcite. Příbram, dump of the shaft No. 16. Width of picture is 2.5 mm.

No. 16. This shaft is localized in the ore deposit Háje, but it was also used as a central shaft for mining of other nearby deposits (Bytíz, Jerusalém). We suppose that the majority of Se-bearing material came from the ore deposit Bytíz, which provided 52 % of the uranium net-production of the whole Příbram uranium and base-metal district. The shaft No. 16 opened mainly the middle and the deeper parts of the vein system (from 500 m down to the depth of 1800 m under the surface). The deposit was discovered in 1947 and the underground mining of uranium in the Příbram area proceeded from 1948 to 1991 (Ettler et al. 2010).

Antimonselite was found in two samples of carbonate vein containing uraninite with partially different association. On the first specimen (labelled "A"), hakite, Se-rich tetrahedrite, Se-rich chalcostibite and chalcopyrite were found in association with antimonselite. The second
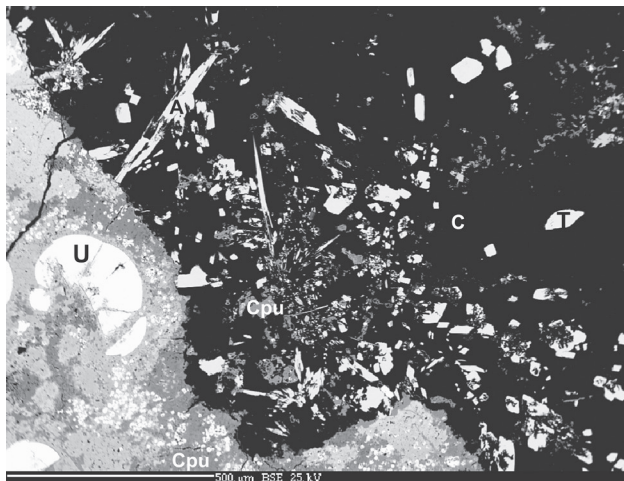

Fig. 2 Back-Scattered Electron image of polished section (specimen A) containing antimonselite (A) in form of light needles and their sections. Dark grains growing in carbonate (C) and darker part of compact ore matrix comprises of chalcopyrite (Cpu) with variable Se content. White globular aggregates in ore matrix are uraninite (U) and light grains in ore matrix are tetrahedrite (T).

specimen ("B") contains antimonselite, hakite, tiemann-ite, permingeatite, clausthalite, Se-rich chalcostibite, an unnamed Se-analogue of chalcostibite, dzharkenite and tetrahedrite.

Antimonselite forms in both samples silver needle-like crystals up to 1.5 mm in length and 0.1 mm in thickness, which occur in calcite gangue. They are visually indistinguishable from stibnite (Fig. 1). The crystals are very brittle, showing a perfect cleavage along {010} and pyramidal termination. Antimonselite is one of the youngest ore mineral phases occurring on both specimens (Fig. 2).

The oldest selenides in association are irregular grains of clausthalite and tiemannite (up to 20–50 μm in size) which are usually overgrown by younger aggregates of hakite, tetrahedrite and Se-rich chalcopyrite (aggregates up to 300 μm in size). The other determined selenides are already distinctly younger. From the younger selenides occurs idiomorphic crystals of dzharkenite up to 50–100 μm; Se-rich chalcostibite as dark silver, very brittle, imperfectly lenticular crystals covering an area of up to 5 mm²; aggregates of perm-ingeatite and an unnamed Se-analogue of chalcostibite with grains up to 20 μm in size.

3. Chemical composition

3.1. Experimental

Quantitative chemical data for the studied samples were obtained by electron microprobe CAMECA SX100 (Laboratory of Electron Microscopy and Microanalysis of Masaryk University and Czech Geological Survey, Brno) in the wavelength-dispersive mode with an accelerating voltage of 25 kV, a specimen current of 10 nA, and a beam diameter of about 1–2 μm. The following standards and X-ray lines were used: Cu (CuK_α), Ag (AgL_α), Au (AuM_α), PbSe (SeL_β), HgTe (HgM_α), FeS$_2$ (SK_α, FeK_α), CdTe (CdL_β), PbS (PbM_α), Sb (SbL_β), pararammelsbergite (AsL_β), ZnS (ZnK_α), Bi$_2$Te$_3$ (TeL_β), Tl(BrI) (TlL_α) and Bi (BiM_β). Peak counting times were 20 s for all elements, and one half of the peak time for each background. Raw intensities were converted to concentrations using automatic PAP (Pouchou and Pichoir 1985) matrix-correction software.

3.2. Results

The results of the electron-probe microanalyses of anti-monselite are given in Tab. 1. Antimonselite of the both types shows rather homogeneous composition, character-ized by the sulfur contents of up to 0.559 *apfu* (Tab. 1). Along with S, only minor contents of Cu up to 0.019

Tab. 1 Chemical composition of antimonselite from Příbram

	mean*	1	2	3	4	5	6	7
Cu	0.09	0.04	0.05	0.07	0.00	0.07	0.26	0.17
Sb	53.83	53.45	52.77	53.94	53.84	54.26	54.12	54.40
Se	41.88	43.56	43.57	41.65	41.62	40.86	40.99	40.92
S	3.16	2.02	2.07	3.23	3.48	3.61	3.84	3.90
Total	98.97	99.07	98.46	98.89	98.95	98.80	99.21	99.39
Cu	0.007	0.003	0.004	0.005	0.000	0.005	0.019	0.012
Sb	2.061	2.082	2.063	2.066	2.051	2.069	2.044	2.051
Cu+Sb	2.068	2.085	2.067	2.071	2.051	2.074	2.063	2.063
Se	2.472	2.616	2.626	2.459	2.445	2.403	2.387	2.379
S	0.460	0.298	0.307	0.470	0.504	0.523	0.551	0.559
Se+S	2.932	2.915	2.933	2.929	2.949	2.926	2.937	2.937

* mean of 7 point analyses; calculation on the basis of 5 *apfu*

apfu) were found. The empirical formula of the studied antimonselite (mean of 7 point analyses, based on 5 *apfu*) is $(Sb_{2.06}Cu_{0.01})_{\Sigma2.07}(Se_{2.47}S_{0.46})_{\Sigma2.93}$.

Among the other determined minerals, tiemannite (Se + Hg + Cu + Cd + Zn + As + Ag + Tl = 2 *apfu*) is a S-free phase with minor contents of Cd (up to 0.03 *apfu*) and Cu (up to 0.05 *apfu*). Clausthalite (Pb + Se + S + Sb + Tl + Bi = 2 *apfu*) is close to end-member with only 0.07 *apfu* S and 0.04 *apfu* Sb. Hakite (Se + Cu + Sb + Hg + S + Zn + Ag + As + Cd = 29 *apfu*) is a Hg-rich phase with various contents of S (0.21–4.43 *apfu*). Tetrahedrite (Se + Cu + Sb + Hg + S + Zn + Ag + As + Cd = 29 *apfu*) has a variable composition; both Fe- and Zn-rich members were found. Selenium content in tetrahedrite varies from 0.01 to 5.83 *apfu*. Chalcopyrite (S + Cu + Fe + Se + Te + As + Ag = 4 *apfu*) is Se-rich (0.18–0.69 *apfu*). Permingeatite (Cu + Sb + Se + Fe = 8 *apfu*) is close to the ideal formula, only with 0.28–0.33 *apfu* S. Se-rich chalcostibite (S + Cu + Sb + Se + Ag + Fe + As + Hg = 4 *apfu*) has 0.36–0.72 *apfu* of Se, and As contents up to 0.06 *apfu*. Unnamed Se-analogue of chalcostibite (S + Cu + Sb + Se + Ag + Fe + As + Hg = *apfu*) is close to end-member $CuSbSe_2$ with only 0.09–0.35 *apfu* S and up to 0.05 *apfu* As. Dzharkenite (Se + Fe + S + Cu + Ag + Hg = 3 *apfu*) is close to the ideal formula $FeSe_2$ with Cu up to 0.02 *apfu* and S in the range of 0.04–0.11 *apfu*.

4. Powder X-ray diffraction

4.1. Experimental

The X-ray powder diffraction pattern of antimonselite was obtained from hand-picked samples by a Bruker D8 Advance diffractometer (National Museum, Prague) with a solid-state 1D LynxEye detector using CuK_α radiation and operating at 40 kV and 40 mA. In order to minimize the background, the powdered sample

was placed on the surface of a flat silicon wafer from acetone suspension. Powder pattern was collected in the Bragg–Brentano geometry in the range 5–72° 2θ, step 0.01° and counting time of 30 s per step (total duration of experiment was *c*. 3 days). Positions and intensities of diffractions were found and refined using the PearsonVII profile-shape function with the ZDS program package (Ondruš 1993) and the unit-cell parameters were refined by the least-squares algorithm implemented by Burnham (1962).

Tab. 2 PXRD data of antimonselite from Příbram

h	k	l	$d_{obs.}$	$d_{calc.}$	$I_{obs.}$	$I_{calc.}$
1	0	1	8.249	8.247	19	6
2	0	0	5.872	5.872	100	14
0	0	2	5.790	5.792	4	4
2	0	1	5.239	5.237	78	41
2	0	2	4.123	4.124	21	6
3	0	1	3.708	3.709	41	18
1	0	3	3.668	3.668	23	12
3	0	2	3.243	3.243	60	45
2	0	3	3.227	3.226	31	12
1	1	2	3.136	3.137	1	71
4	0	0	2.936	2.936	3	1
2	1	2	2.847	2.847	5	100
0	1	3	2.756	2.756	4	62
3	0	3	2.748	2.749	6	3
4	0	2	2.618	2.619	48	48
2	0	4	2.596	2.597	28	15
4	0	3	2.3367	2.3371	5	4
3	0	4	2.3288	2.3282	11	7
1	0	5	2.2730	2.2731	3	3
5	0	2	2.1763	2.1766	15	12
2	0	5	2.1555	2.1552	12	16
4	0	4	2.0616	2.0618	10	5
3	0	5	1.9941	1.9939	20	14
6	0	0	1.9570	1.9573	8	2
0	0	6	1.9304	1.9308	5	3
6	0	1	1.9304	1.9299	5	2
1	0	6	1.9058	1.9052	3	6
6	1	0	1.7531	1.7525	2	43
6	0	3	1.7455	1.7458	6	12
4	0	6	1.6130	1.6132	5	4
2	0	7	1.5930	1.5929	7	13
7	0	3	1.5391	1.5387	7	6
6	0	5	1.4955	1.4952	19	6
2	2	5	1.4533	1.4532	1	9
7	0	4	1.4520	1.4517	7	4
8	0	2	1.4228	1.4230	2	2
4	1	7	1.3537	1.3537	3	17
8	0	4	1.3091	1.3094	2	1

Tab. 3 Refined unit-cell parameters of antimonselite

	Příbram; this paper (powder)	Příbram; this paper (single-crystal)	China, Bentou Min et al. (1998)	China, Kaiyang Chen et al. (1993)
a	11.7437(6)	11.7156(3)	11.744(4)	11.747
b	3.9358(7)	3.9514(11)	3.955(2)	3.984
c	11.5846(8)	11.5645(3)	11.588(5)	11.593
V	535.4(1)	535.36(15)	538.23	542.6

4.2. Results

Experimental X-ray powder diffraction pattern of antimonselite from Příbram has peak intensities distinctively different from theoretical values calculated from the single-crystal study results. Intensities of some diffractions are an order of magnitude lower (20–70×) than theoretical values (Tab. 2). Besides minimal amount of available material, this is probably caused also by the preferred orientation, produced by the perfect cleavage of the mineral and its needle to fibrous character (Toraya and Marumo 1981). Similar effect was described recently e.g. in case of extremely fibrous mimetite from Jáchymov (Sejkora et al. 2011b) or acicular to fibrous

marrucciite crystals from Gelnica (Sejkora et al. 2011a). The other published antimonselite PXRD data (Liu et al. 1999, 2008) do not show any preferred orientation probably due to predominant granular shape of the studied crystals. The unit-cell parameters were refined from powder diffraction pattern of antimonselite from Příbram as $a = 11.7437(6)$, $b = 3.9358(7)$, $c = 11.5846(8)$ Å, $V = 535.4(1)$ Å^3. Our data are in good agreement with the published ones (Tab. 3).

5. Crystal structure

5.1. Experimental

A long-prismatic blackish single crystal of antimonselite, with the dimensions $0.29 \times 0.03 \times 0.02$ mm, was selected under the optical stereomicroscope for collection of the 3-D intensity data. They were aquired by Oxford Diffraction Gemini single-crystal diffractometer system, equipped with the Atlas CCD area detector, using monochromatized MoK_α radiation from sealed tube, $\lambda = 0.71073$ Å, and with a fibre-optics Mo-Enhance collimator. The unit cell was refined by a least-squares algorithm of the CrysAlis Pro Package (Agilent Technologies 2012) from 3353 reflections and gave orthorhombic unit cell with $a = 11.7156(3)$, $b = 3.9514(11)$, $c = 11.5645(3)$ Å, $V = 535.36(15)$ Å^3, and $Z = 4$. In order to obtain better resolution of overlapping reflections, originating from the split crystals of antimonselite, the detector-to-crystal distance was set up to 120 mm. The ω rotational scans (frame width of 0.8° and 55 s exposure per frame) were used to collect the full-sphere data. In total, 6404 reflections were measured. After merging symmetrically equivalent reflections, 677 unique and 634 observed reflections, with the criterion [$I_{obs} > 3\sigma(I)$], were

Tab. 4 Crystallographic data and refinement parameters for antimonselite

Structural formula	Sb$_2$(Se$_{2.577}$S$_{0.423}$)
Crystal data	
Space group	*Pnma*
a [Å]	11.7156(3)
b [Å]	3.9514(11)
c [Å]	11.5645(3)
V [Å^3]	535.36(15)
Z	4
D$_{calc}$ [g.cm^{-3}]	5.706
Data collection	
Temperature	300K
Detector; wavelength	Atlas CCD; MoK_α (0.71073 Å)
Crystal dimensions	$0.29 \times 0.03 \times 0.02$ mm
Collection mode	ω scans, full sphere
Limiting θ angles	4.94–27.51°
Limiting Miller indices	$-15<h<14, -5<k<4, -14<l<14$
No. of reflections	6406
No. of unique reflections	677
No. of observed reflections (criterion)	634 [$I_{obs}>3\sigma(I)$]
R$_{int}$, coverage	0.0237, 98.99%
Absorption correction (mm^{-1}), T$_{min}$/T$_{max}$	27.54, analytical, 0.103/0.548
F$_{000}$	786
Refinement by Jana2006 on F^2	
Parameters refined, constraints, restraints	31, 0, 18
R$_1$, wR$_2$ (obs)	0.0143, 0.0360
R$_1$, wR$_2$ (all)	0.0166, 0.0369
GOF obs/all	1.21/1.20
Δρ$_{min}$, Δρ$_{max}$ (eÅ^{-3})	–0.50, 0.53
Weighting scheme, details	σ, $w = 1/(\sigma^2(I) + 0.0004I^2)$

Tab. 5 Atomic positions, equivalent and harmonic displacement parameters

	Occ.*	x	y	z	U_{eq}	U_{11}	U_{22}	U_{33}	U_{12}	U_{13}	U_{23}
Sb1		0.03043(3)	0.25	0.67259(3)	0.023137(10)	0.02316(18)	0.01707(17)	0.02387(19)	0	0.00199(12)	0
Sb2		0.35295(3)	0.25	0.46142(3)	0.02450(11)	0.02200(18)	0.02175(18)	0.0298(2)	0	0.00451(13)	0
Se1	0.896(4)	0.21386(4)	0.25	0.80574(4)	0.01928(16)	0.0211(3)	0.0180(3)	0.0187(3)	0	−0.00122(18)	0
S1	0.104(4)										
Se2	0.879(4)	0.37113(4)	0.25	0.05587(4)	0.01902(16)	0.0219(3)	0.0171(3)	0.0181(3)	0	0.00255(18)	0
S2	0.121(4)										
Se3	0.802(4)	0.05366(4)	0.25	0.12853(5)	0.01905(17)	0.0205(3)	0.0157(3)	0.0210(3)	0	0.0002(2)	0
S3	0.198(4)										

* occupational factors

Se/S atoms constrained to have equal coordinates and atomic displacement parameters

Tab. 6 Interatomic distances (in Å) and bond-valence sums (in valence units) for the antimonselite structure

Sb1–Se1/S1	2.6437(6)		$\sum$BV
Se2/S2	2.6562(9) (2×)	Sb1	2.791(3)
Se2/S2	3.2347(61)	Sb2	2.710(3)
Se3/S3	3.1881(9) (2×)	Se1	2.101(2)
Sb2–Se1/S1	2.7852(9) (2×)	Se2	2.092(3)
Se2/S2	3.4624(8) (2×)	Se3	2.220(2)
Se3/S3	2.9724(9) (2×)		
Se3/S3	2.5713(6)		

The bond-strength parameters used in calculations for Sb–Se pair after Brown (2013, pers. comm.)

obtained. Data were corrected for background, Lorentz effect and polarization (CrysAlis Pro RED; Agilent Technologies 2012), and a combined correction for absorption was applied (multi-scan and analytical correction, the latter after Clark and Reid 1995), leading to an internal *R*-factor of the merged dataset equal to 0.0237.

5.2. Structure solution and refinement

Crystal structure of antimonselite was solved by the charge-flipping algorithm implemented in the Superflip program (Palatinus and Chapuis 2007) and refined by the full-matrix least-square algorithm of the Jana2006 program (Petříček et al. 2006) based on F^2. The space group *Pnma* was chosen based on the reflection statistics and this choice was also indicated by the Superflip program output. No cell of the higher symmetry was found using LePage and ADDSYMM (Spek 2003, 2009). In the previous structure determinations (Min et al. 1998), a different space-group setting was used. It was, however, not consistent with the conventional setting of the isotypic stibnite, having *Pnma*. All the 5 atoms in the asymmetric unit were found by the structure solution. The subsequent refinement including anisotropic displacement parameters of all atoms and refined site-occupancies converged to the final residuals $R_1 = 0.0143$ for 634 unique observed and $wR_2 = 0.0369$ for all 677 reflections with a $GOF_{all} = 1.20$ (Tab. 4). The difference Fourier maps did not reveal any significant residual electron density; the highest positive maximum was 0.53 eÅ^{-3}, located 1.00 Å from the Sb1

atom.[1] Crystallographic parameters and data collection details are listed in Tab. 4. Final atom coordinates and displacement parameters are given in Tab. 5. The structural formula of the crystal studied by single-crystal X-ray diffraction obtained from the site-scattering refinement is $Sb_2(Se_{2.577}S_{0.423})$, which is satisfactorily matching the results of the electron-microprobe study. The results of the bond-valence analysis of the structure are listed in Tab. 6, along with the interatomic distances.

6. Discussion

Antimonselite, stibnite and their intermediate members are known from several gold and uranium deposits in China. Based on average electron-microprobe analyses of Sb_2Se_3–Sb_2S_3 from the Laerma and Qiongmo localities (China), the formulae of Se-bearing stibnite, selenium stibnite, sulfur antimonselite and S-bearing antimonselite can be written as $Sb_{2.03}(S_{2.67}Se_{0.33})_{3.00}$, $Sb_{2.00}(S_{2.06}Se_{0.94})_{3.00}$, $Sb_{1.98}(Se_{1.71}S_{1.31})_{3.00}$ and $Sb_{1.86}(Se_{2.64}S_{0.36})_{3.00}$, respectively (Liu et al. 1999). According to this nomenclature, it is possible to classify antimonselite from Příbram as S-bearing antimonselite. Differences between analyses of antimonselite from Příbram and other analyses of stibnite–antimonselite series, both synthetic and natural (Fig. 3), are caused by lower than ideal ratio of sum of anions versus sum of cations.

The overall rarity of antimonselite is probably related to specific mode of origin of this mineral phase. The well documented minerals of the stibnite–antimonselite series from the stratabound gold deposits Laerma and Qiongmo

---

[1] The residual density, which is also responsible for the higher goodness of fit (GOF) may be connected with absorption correction, unresolved twinning features (the small number of overlapping reflections) or bonding effects.
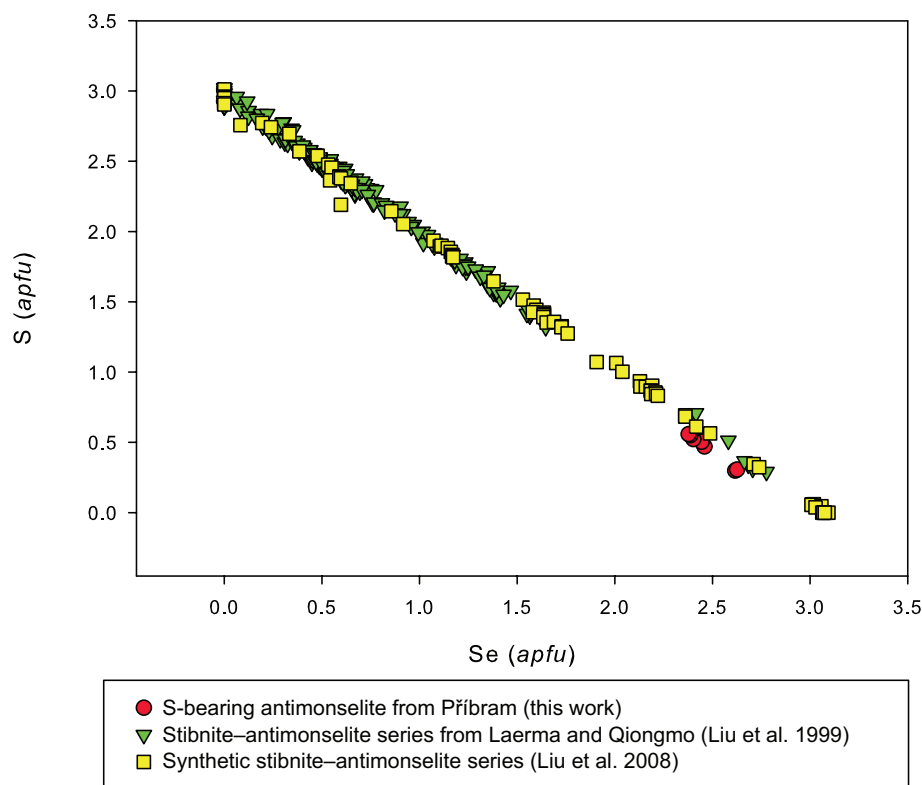
Fig. 3 Plot of Se and S contents (apfu) of natural stibnite–antimonselite series from Příbram (this work), Laerma and Qiongmo in China (Liu et al. 1999) and synthetic stibnite–antimonselite series (Liu et al. 2008).

were supposed to have crystallized at 150–210 °C (Liu et al. 1999). The U mineralization in Příbram is characterized by temperatures between 200 and 80 °C, but the deposition of uranium minerals, which are in direct association with younger selenides mineralization, preceded at temperatures between 130–80 °C (Žák and Dobeš 1991). The extensive group of selenides of many elements like Pb, Sb, Ag, Hg, Cu and Tl found in many types of gangue material of the Příbram uranium and base-metal deposit indicates variable conditions of origin. This is supported by the joint occurrence of selenide–sulfide pairs at the uraninite stage (e.g. hakite–tetrahedrite, chalcopyrite–eskebornite, tiemannite–cinnabar, antimonselite–stibnite and others), which were also described on the original Chinese localities. The most interesting Se minerals in studied Příbram specimens, including antimonselite, were found in the youngest parts of the uranium–carbonate stage. These parts were formed by hydrothermal alteration of the older gangue filling, accompanied by the origin of younger uraninite, antimonselite and other sulfides and selenides. The observed association in the specimen "B": tiemannite–hakite–tetrahedrite–antimonselite, shows the decreasing activity of Se in hydrothermal solutions accompanied by the crystallization of Hg or Cu–Hg selenides and terminated by the crystallization of Se-poor tetrahedrite. The presence of the youngest antimonselite in this association is a clear evidence for infiltration of rejuvenated solutions with high selenium activity.

References

AGILENT TECHNOLOGIES (2012) CrysAlis CCD and CrysAlis RED. Oxford Diffraction Ltd, Yarnton, Oxfordshire, UK

BURNHAM CW (1962) Lattice constant refinement. Carnegie Institute Washington Yearbook 61: 132–135

CHEN L, ZHANG Q, LI D, WANG G (1993) Antimonselite, a new mineral. Acta Miner Sinica 13: 7–11 (in Chinese)

CLARK RC, REID JS (1995) The analytical calculation of absorption in multifaceted crystals. Acta Cryst A51: 887–897

DYMKOV JM (1985) Selenides of uraninite–carbonate veins. In: Paragenesis of the Minerals of the Uranium-Bearing Veins. Nedra, Moscow, pp 153–162 (in Russian)

ETTLER V, SEJKORA J, DRAHOTA P, LITOCHLEB J, PAULIŠ P, ZEMAN J, NOVÁK M, PAŠAVA J (2010) Příbram and Kutná Hora mining districts – from historical mining to recent environmental impact. In: IMA 2010, Budapest. Acta Miner-Petrol, Field Guide Series 7: 1–23

Litochleb J, Sejkora J, Šrein V (2004) Selenide minerals from the Bytíz deposit (Příbram uranium–base-metal ore district). Bull miner-petrolog Odd Nár Muz (Praha) 12: 113–123 (in Czech)

Liu J, Liu J, Lu W, Zheng M, Zhou Y, Gu X, Zhang B (1998) Se-stibnite from Qiongmo gold deposit in Western Qinling, China. Acta Miner Sinica 18: 445–451(in Chinese)

Liu J, Liu J, Liu C, Lu W, Liu S, Su W (1999) Mineralogy of the stibnite–antimonselite series. Int Geol Rev 41: 1042–1050

Liu J, Liu J, Li J, Xie H, Wang J, Deng J, Feng C, Qi F, Zhang N (2008) Experimental synthesis of the stibnite–antimonselite solid solution series. Int Geol Rev 50: 163–176

Min M, Wu J (1992) Stable isotopes studies of paleokarst-hosted uranium deposits in China. Geoch J 32: 103–115

Min M, Li D, Shi N, Liu Q, Cao Y (1995) Some new data on antimonselite. Acta Miner Sinica 15: 303–304

Min M, Zhai J, Wang X, Shen B, Wen G, Fan T (1998) Refinement of the crystal structure for a new mineral – antimonselite. Chinese Sci Bull 43: 413–416

Ondruš P (1993) A computer program for analysis of X-ray powder diffraction patterns. Materials Sci Forum, EPDIC-2, Enchede, 133-136: 297-300.

Palatinus L, Chapuis G (2007) Superflip – a computer program for the solution of crystal structures by charge flipping in arbitrary dimensions. J Appl Crystallogr 40: 451–456

Petříček V, Dušek M, Palatinus L (2006) Jana2006. The crystallographic computing system. Institute of Physics, Prague, Czech Republic (*http://jana.fzu.cz*)

Pouchou JL, Pichoir F (1985) "PAP" ($\varphi \rho Z$) procedure for improved quantitative microanalysis. In: Armstrong JT (ed) Microbeam Analysis. San Francisco Press, San Francisco, pp 104–106

Růžička J (1986) Minerals of the Příbram Uranium Deposit. Komitét sympozia Hornická Příbram ve vědě a technice. Příbram, pp 1–244 (in Czech)

Sejkora J, Ozdín D, Laufek F, Plášil J, Litochleb J (2011a) Marrucciite, a rare Hg sulfosalt from the Gelnica ore deposit (Slovak Republic), and its comparison with the type occurrence at Bucca della Vena mine (Italy). J Geosci 56: 399–408

Sejkora J, Plášil J, Císařová I, Škoda R, Hloušek J, Veselovský F, Jebavá I (2011b) Interesting supergene Pb-rich mineral association from the Rovnost mining field, Jáchymov (St. Joachimsthal), Czech Republic. J Geosci 56: 257–271

Spek AL (2003) Single-crystal structure validation with the program PLATON. J Appl Cryst 36: 7–13

Spek AL (2009) Structure validation in chemical crystallography. Acta Cryst D65: 148–155

Škácha P, Sejkora J (2007) The occurrence of arsenolamprite at the Příbram uranium–polymetallic district (Czech Republic). Bull mineral-petrolog Odd Nár Muz (Praha) 14–15: 131–133 (in Czech with English abstract)

Škácha P, Sejkora J, Litochleb J, Hofman P (2009) The occurrence of cuprostibite in the Příbram uranium–base metals ore district (the shaft 16, Příbram–Háje), Czech Republic. Bull miner-petrolog Odd Nár Muz (Praha) 17: 73–78 (in Czech with English abstract)

Škácha P, Vlček V, Sejkora J, Plášil J, Goliáš V (2010) Compositional trends in hakite, possible discrepancies from ideal structure. Acta Miner-Petrol, Abstract Series 6: 725

Škácha P, Buixaderas E, Plášil J, Sejkora J, Goliáš V, Vlček V (2014) Permingeatite, Cu_3SbSe_4, from Příbram (Czech Republic): description and Raman spectroscopy investigations of the luzonite-group of minerals. Canad Mineral 52: 501–511

Toraya H, Marumo F (1981) Preferred orientation correction in powder pattern fitting. Mineral J 10: 211–221

Tvrdý J (2003) Geology and ore veins of the Příbram district. Lapis 7/8: 23–26 (in German)

Wen H, Carignan J, Qiu Y, Liu S (2006) Selenium speciation in Kerogen from two Chinese selenium deposits: environmental implications. Environ Sci Technol 40: 1126–132

Žák K, Dobeš P (1991) Stable isotopes and fluid inclusions in hydrothermal deposits: the Příbram ore region. Rozpr Čs Akad Věd, Ř mat přír Věd, Academia, Prague, pp 1–109